Conduction mechanisms in biphenyl dithiol single-molecule junctions

M. Bürkle,[1,2] J. K. Viljas,[3,4] D. Vonlanthen,[5] A. Mishchenko,[6] G. Schön,[1,2,7] M. Mayor,[2,5,7,*] T. Wandlowski,[6,†] and F. Pauly[1,2,8,‡]

[1]*Institute of Theoretical Solid State Physics, Karlsruhe Institute of Technology, D-76131 Karlsruhe, Germany*

[2]*Center for Functional Nanostructures, Karlsruhe Institute of Technology, D-76131 Karlsruhe, Germany*

[3]*Low Temperature Laboratory, Aalto University, P.O. Box 15100, FIN-00076 AALTO, Finland*

[4]*Department of Physics, P.O. Box 3000, FIN-90014 University of Oulu, Finland*

[5]*Department of Chemistry, University of Basel, CH-4003 Basel, Switzerland*

[6]*Department of Chemistry and Biochemistry, University of Bern, CH-3012 Bern, Switzerland*

[7]*Institute of Nanotechnology, Karlsruhe Institute of Technology, D-76344 Eggenstein-Leopoldshafen, Germany*

[8]*Molecular Foundry, Lawrence Berkeley National Laboratory, Berkeley, California 94720, USA*

(Received 1 September 2011; revised manuscript received 16 December 2011; published 21 February 2012)

Based on density-functional theory calculations, we report a detailed study of the single-molecule charge-transport properties for a series of recently synthesized biphenyl-dithiol molecules [D. Vonlanthen *et al.*, Angew. Chem., Int. Ed. **48**, 8886 (2009); A. Mishchenko *et al.*, Nano Lett. **10**, 156 (2010)]. The torsion angle φ between the two phenyl rings, and hence the degree of π conjugation, is controlled by alkyl chains and methyl side groups. We consider three different coordination geometries, namely, top-top, bridge-bridge, and hollow-hollow, with the terminal sulfur atoms bound to one, two, and three gold surface atoms, respectively. Our calculations show that different coordination geometries give rise to conductances that vary by one order of magnitude for the same molecule. Irrespective of the coordination geometries, the charge transport calculations predict a $\cos^2\varphi$ dependence of the conductance, which is confirmed by our experimental measurements. We demonstrate that the calculated transmission through biphenyl dithiols is typically dominated by a single transmission eigenchannel formed from π electrons. For perpendicular orientation of the rings a residual conductance arises from σ-π couplings. But only for a single molecule with a completely broken conjugation we find a nearly perfect degeneracy of the σ-π eigenchannels for the hollow-hollow-type contact in our theory.

DOI: 10.1103/PhysRevB.85.075417 PACS number(s): 73.63.Rt, 85.65.+h, 73.23.Ad, 31.15.es

I. INTRODUCTION

After the first realizations of single- or few-molecule contacts,[1–3] a major theme of research represents the controlled fabrication of molecular junctions with desired properties. As an example, several groups demonstrated recently that the conductance of junctions containing biphenyl derivatives can be controlled by the torsion angle φ between the two phenyl rings.[4–6] However, not only has the investigation of the conductance of more complex molecules become feasible,[7–9] but also the study of additional aspects such as the signature of molecular vibrations in the electric current,[10] current-induced heating,[11,12] and distinction of electron or hole conduction by measurement of the thermopower.[13] Furthermore, information on individual conduction channels can be obtained by use of superconducting electrodes[14] or shot-noise measurements.[15] All these advances allow for a better characterization of the single-molecule charge transport when compared with theory.

Despite experimental and theoretical achievements, measurement and modeling of electron transport in molecular junctions are still challenging tasks. This is mainly due to the observed variability in junction conductances and the corresponding statistical nature of the experiments.[3,16,17] In this regard, calculations based on the approximate density functional theory (DFT) can be helpful to obtain a better understanding of the charge transport mechanisms involved and to interpret trends in the experimental data based on computed structure-transport relationships. In agreement with the experimental observations, they show, in particular, that the electric conduction strongly depends on the molecular conformation[4–6,18–23] and the precise geometry in the single-molecule junctions.[24–28]

In our recent studies,[5,29] we have explored the conduction properties of biphenyl-dithiol (BPDT) molecules bound to Au electrodes. For these molecules, named here M0–M7 and displayed in Fig. 1, the molecular conjugation is gradually varied by the use of alkyl chains and methyl side groups. In this follow-up paper, we present a more detailed theoretical analysis of their transport properties based on DFT calculations. We study an extended, systematic set of contact geometries and place special emphasis on transport for perpendicular ring orientations. The conduction mechanisms are revealed by means of a tight-binding model (TBM),[20,30] the more frequently used Lorentz model (LM),[31] and the eigenchannel decomposition of the conductance.[32] The TBM accounts only for the π orbitals of the BPDTs, which are typically the most relevant electronic states for the charge transport through such conjugated organic molecules. By fitting the transmission curves computed within DFT to the TBM expressions, effective parameters for the electronic structure of the π electron system are extracted. The complexity of the TBM is reduced further in the LM. In the form applied here, it considers only the transmission resonances of the highest occupied molecular orbital (HOMO) and the lowest unoccupied molecular orbital (LUMO), which are both assumed to be of a Lorentzian form. Finally, the eigenchannel decomposition of the conductance, based on the DFT results, allows us to study the validity of these simplified models, and transmission eigenchannel wave functions offer an intuitive visual interpretation of the complicated numerical results. Our analysis suggests that the coordination site ("top,"

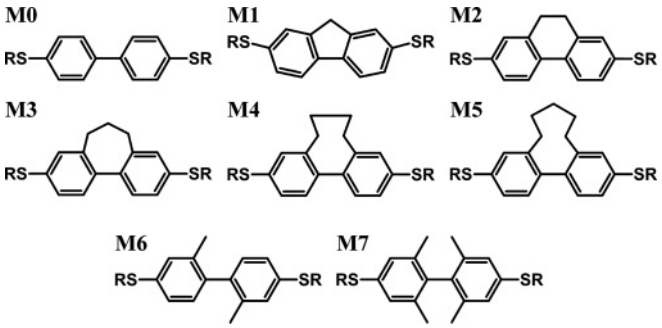

FIG. 1. Chemical structure of the investigated molecules. "S" is the sulfur atom, and "R" represents the acetyl group for the synthesized form of the molecules, a hydrogen atom after the *in situ* deprotection, or the Au electrode for the transport measurements.

"bridge," or "hollow") of the anchoring sulfur atom at the Au surface plays a decisive role in conduction through the molecular junction.

The paper is organized as follows. In Sec. II we briefly summarize key experimental findings.[5,29] Technical aspects of the DFT and transport calculations are discussed in Sec. III. Studies of the dependence of junction conductance on the torsion angle and the substrate-adsorbate coordination geometry are presented and analyzed in Sec. IV. The main text ends with a summary and conclusions in Sec. V. The appendices contain details on the methods used to analyze the DFT results in Sec. IV. Thus, in Appendix A we explain our scheme to construct transmission eigenchannel wave functions without the need to resort to Löwdin transformations when nonorthogonal, local basis sets are used in the DFT calculations. Finally, Appendix B discusses the relation between the TBM and the LM.

II. EXPERIMENTS

We synthesized the BPDT molecules M0–M7 of Fig. 1 with acetyl-protected terminal thiol groups, i.e., R = $COCH_3$.[29,33–35] The torsion angle φ between the phenyl rings is gradually varied by introduction of alkyl side chains of variable length or methyl groups.[5,29] This leaves the length of the molecule unchanged. The torsion angles were determined by an x-ray structure analysis of single crystals formed from each of these compounds, except for M0.

This systematic set of molecules exhibits several remarkable features in single-molecule transport measurements, which we examine further below. First, stable junctions can be formed with gold leads by the terminal sulfur atoms after deprotection. Second, the conformation of the biphenyls is efficiently locked by the alkyl chains and the steric hindrance of the methyl side groups. Variations of torsion angles are hence expected to be low.[19,36,37] Third, strongly electron-donating or electron-withdrawing side groups are avoided, which have been demonstrated to influence noticeably the single-molecule transport.[38]

We studied the conductance of single-molecule junctions by means of a scanning-tunneling-microscopy-break-junction method (see Ref. 5). The experiments were carried out at a solid liquid interface under ambient conditions in a solution of 1,3,5-trimethylbenzene and tetrahydrofuran at a mixing

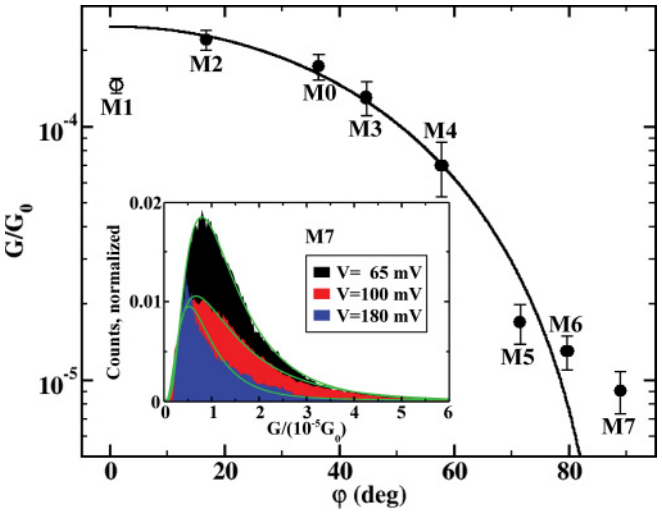

FIG. 2. (Color online) Dependence of the experimental conductance G (points) on the torsion angle φ for M0–M7 with φ determined from x-ray structures. The solid line represents a fit to $G = a\cos^2\varphi$ with $a = 2.49 \times 10^{-4} G_0$. The inset shows conductance histograms for M7, obtained at three different bias voltages. The typical single-molecule conductance (corresponding to a point in the main panel) is obtained as the average of the peak positions of the fitted log-normal distributions at the three different biases, and error bars are determined from the peak variations. For M7 this yields $G = (9 \pm 2) \times 10^{-6} G_0$.

ratio of 4:1, containing 0.15 mM of the respective BPDT derivatives. The substrate was a flame-annealed, atomically flat Au ⟨111⟩ single crystal. The gold tip was electrochemically etched, revealing a sharp apex, capable of molecular resolution imaging. We recorded several thousand current-distance traces representing the breaking of gold substrate-molecule-gold tip junctions. The statistical analysis of these traces led to conductance histograms, as illustrated for M7 in the inset of Fig. 2. Further details of the experimental conditions and data analysis have been presented in Refs. 5 and 17. The most probable or "typical" molecular junction conductance is determined as an average of the peak values in the conductance histograms, measured at three different bias voltages (see Fig. 2, inset).[39]

When we plot this typical conductance as a function of the torsion angle on a linear scale, we find a $G = a\cos^2\varphi$ dependence with $a = 2.49 \times 10^{-4} G_0$, as expected for off-resonant π-dominated charge transport.[5,19] Here $G_0 = 2e^2/h$ is the conductance quantum. Figure 2 shows a semilogarithmic plot of G versus φ. The graph reveals several distinct features. The conductance of M1 is lower than expected from the general trend. We observed a similar exceptional behavior of M1 in a recent investigation of cyano-terminated molecules (i.e., S is replaced by CN in Fig. 1),[6] showing, however, a higher value than expected, and these irregularities are currently of an unclear origin. On the other hand, there are deviations from the $\cos^2\varphi$ law for the larger torsion angles for molecules M5, M6, and M7. While the measured conductance of M5 is too low, those of M6 and M7 with $\varphi \gtrsim 80^\circ$ are above the $\cos^2\varphi$ curve. A simple π-orbital model[20,30] loses its validity for large torsion angles, and any other than π-π couplings prevent the complete suppression of transport. We show below that the

residual couplings are of π-σ type. Given some uncertainties with respect to the torsion angles for M5 and M6 as discussed below (see Sec. IV A), the measurement point for M7 is the clearest evidence of such a residual conductance for nearly perpendicular ring orientations. Note also the conductance histograms in the inset of Fig. 2, which clearly indicate a nonvanishing typical conductance value for M7.

We observe that the conductance histograms, such as those shown in the inset of Fig. 2, are asymmetric with a long tail toward higher conductance values. The broad tail region could be related to junctions with multiple molecules, modifications in substrate-adsorbate coordination from junction to junction, atomic rearrangements upon stretching, local surface roughness, or electrode-induced changes of the average torsion angle due to charge transfer and geometric constraints. In contrast to results for biphenyl-diamines,[4] we do not observe clear correlations between the full-widths-at-half-maximum of the conductance peaks and the expected differences in torsion-angle-related energy barriers of the various BPDTs studied.[6,19] If a substantial part of the experimental conductance scatter would be due to the variation of the torsion angle of the biphenyl core, then M0 with a low energy barrier for ring rotation of about 0.1 eV[19] should exhibit a particularly broad conductance distribution. However, we see no evidence to support this hypothesis. In agreement with conclusions from other works[36] we propose that the use of thiol anchoring groups leads to the variation of the single-molecule conductance being dominated by changes in the metal-molecule contact.

III. THEORETICAL PROCEDURES

A. Electronic structure and geometry optimization

Electronic structure calculations and geometry optimizations are performed within DFT. We use the quantum chemistry package TURBOMOLE 6.2.[40] For all calculations, we employ the standard basis set, def-SV(P), which is of split-valence quality with polarization functions on all nonhydrogen atoms.[41–43] We treat all molecules and contact geometries as open-shell systems with no unpaired electrons and use BP86 as the exchange-correlation functional.[44,45] Total energies are converged to a precision of better than 10^{-6} a.u., and geometry optimizations are carried out until the change of the maximum norm of the Cartesian gradient is below 10^{-4} a.u.

B. Charge transport calculations

We determine conduction properties within the Landauer-Büttiker formalism.[46] The energy-dependent transmission $\tau(E)$ is expressed using standard Green's function techniques (see also Appendix A). The conductance at low temperatures is then given by

$$G = G_0 \tau(E_F) = G_0 \sum_n \tau_n(E_F), \qquad (1)$$

with τ_n being the transmission probability of the transmission eigenchannel n.

In the calculations we model the electrodes of a molecular junction as perfect semi-infinite crystals to the left and to the right. The molecule is connected to their surface by atomically sharp metal tips. We describe this by computing a finite "extended central cluster" (ECC), as displayed in Fig. 3, into which large parts of the metal electrodes are included to ensure the proper alignment of molecular levels with respect to E_F.

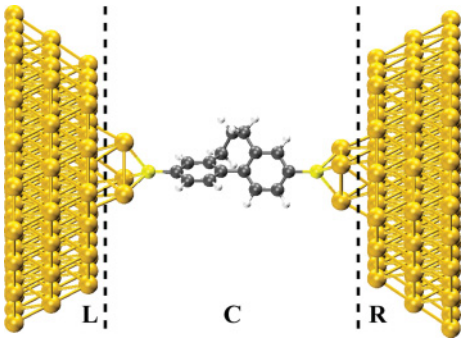

FIG. 3. (Color online) Division of the ECC into the L, C, and R regions. A large number of gold atoms (around 120 in L and R, respectively) is used to represent the electrodes in the DFT calculations.

Due to the locality of the Gaussian basis sets employed, we are able to partition the ECC into three subsystems, formed from basis states in the left (L), central (C), and right (R) parts. The atoms in the L and R regions of the ECC are assumed to represent that part of the semi-infinite crystal surface that couples to C. We extract the parameters for a description of region C and its coupling to the left and right electrode surfaces from the electronic structure of the ECC. On the other hand, the surface Green's functions of the L or R electrodes are constructed using parameters obtained from a spherical Au cluster of several hundred atoms. This calculation yields a Fermi energy of $E_F = -5.0$ eV. With these ingredients, we compute the transmission probability $\tau(E)$. A more detailed description of our cluster-based density-functional approach to quantum transport can be found in Ref. 47.

In transport experiments with single molecules, often only the low-bias conductance, proportional to the sum of the τ_n in Eq. (1), is measured. However, also the individual τ_n can be resolved.[14,15] On the theory side, in addition to the transmission probabilities of the conduction eigenchannels, also the projection of their wave function onto the central region can be obtained from quantities at hand in the Green's function formalism.[32,48] In order to construct energy-normalized transmission eigenchannel wave functions, which can be compared to each other, we proceed along the lines of Ref. 32. Our efficient procedure, which avoids the Löwdin transformation of Ref. 32, is presented in detail in Appendix A.

C. Contact geometries

The statistical nature of the single-molecule conductance experiments (see Sec. II) does not provide an *a priori* assignment of representative junction geometries. Therefore, we have decided to study three contact structures with different coordinations of the terminal sulfur atoms. The procedure adopted to determine the structure of the ECC is summarized in Fig. 4.

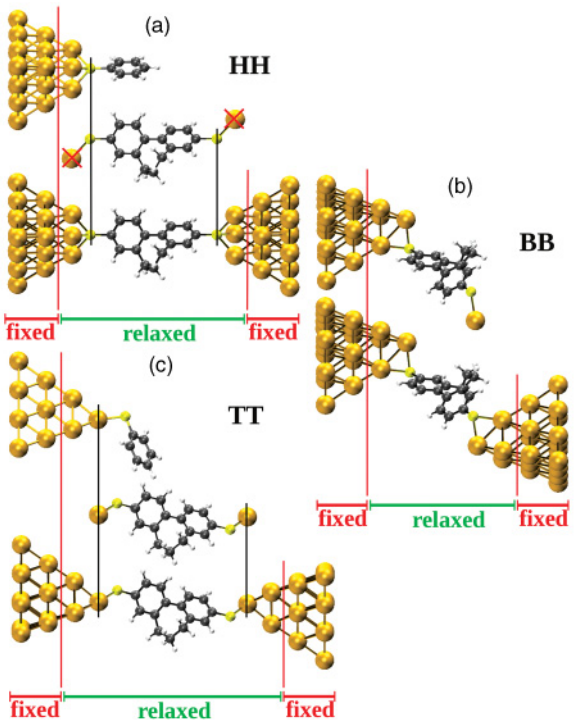

FIG. 4. (Color online) Procedure used to set up the contact geometries for (a) HH, (b) BB, and (c) TT binding, respectively.

In order to model the molecular junctions, we connect the molecule to two Au ⟨111⟩ pyramids, both stemming from the same ideal fcc Bravais lattice. We consider the following three types: For hollow-hollow (HH) [Fig. 4(a)] the S atoms of the molecule are bound at each side to three Au atoms, for bridge-bridge (BB) [Fig. 4(b)] to two Au atoms, and for top-top (TT) [Fig. 4(c)] to only a single Au atom.

For the determination of the HH and TT geometries, we start from the gas-phase structure of each molecule (with SR = H in Fig. 1), replace the terminal H atoms by an S-Au_1 group (R = Au_1 in Fig. 1), and compute ground-state geometries. For HH contacts, the Au_1 atoms are removed. An Au_{19} cluster, resembling a Au ⟨111⟩ pyramid with a thiolated benzene attached, is computed separately. The cluster is positioned at each side of the BPDT such that the S atoms on top of the pyramids coincide with the S atoms of the molecule [Fig. 4(a)]. To obtain the TT geometries, the molecule is oriented such that each Au_1 atom coincides with a tip atom of the Au_{20} pyramids [Fig. 4(c)]. To determine the equilibrium structure for both HH and TT, the inner part is relaxed, and only the two outermost gold layers, consisting of six and ten atoms, are kept fixed in the ideal Au fcc structure.

For the BB geometries we follow slightly different steps. First the terminal H atoms of the gas-phase molecules (with SR = H in Fig. 1) are replaced with S, one side is connected to a Au_{20} pyramid in bridge position, while the other one is terminated with Au_1. The outermost gold layers of the pyramid are kept fixed, while the rest is optimized. A second Au_{20} pyramid is finally added to the Au_1-terminated side, where the relative distances of the binding S atom with respect to the new Au_{20} cluster are chosen to be the same as for the S atom in bridge position at the Au_{20}-terminated side [Fig. 4(b)]. Fixing again only the two outermost Au layers, the structure is optimized to determine the ground-state geometry.

We note that the contact geometries do not only differ with respect to the coordination of the sulfur atoms to the gold electrodes, but also in the stress exerted on the molecules. As visible in Fig. 4(a), the ⟨111⟩ direction is located in the ring plane of a monothiolated benzene molecule on top of the Au_{19} pyramid. Since the S-S axis is along the same direction, the BPDT molecule is expected to adopt a minimum-energy configuration inside the HH junction with φ close to its gas-phase angle. In contrast, in the TT geometries the biphenyl derivative bridges the gold tip atoms, which are opposite to each other. In this case the sulfur atoms are deflected from their equilibrium positions, which would be located along the ⟨111⟩ direction on top of the Au_{20} pyramids [Fig. 4(c)]. In the geometry optimizations we find that the phenyl ring planes of the biphenyl molecules tend to align parallel to the surfaces of the pyramids. Since this may not be possible on both sides of the junction, some torque is exerted. Beside effects related to charge transfer, which may also be present for the HH contacts, geometric constraints thus yield an additional contribution to the change of the torsion angle. Similar effects as for TT are also present for the BB contacts, since the orientations of the phenyl rings with respect to the gold pyramids on both sides are generally different according to our construction.

We have determined binding energies by subtracting the total energy of the contact geometries from those of the frozen separate parts, namely, the left and right Au clusters and the S-terminated biphenyl (without hydrogen on the sulfur atoms). With this procedure, we find the following averaged binding energies for the set of molecules: 5.9 ± 0.3 eV (HH), 2.9 ± 0.2 eV (BB), and 2.2 ± 0.2 eV (TT). Hence, we find a trend of decreasing binding energies with decreasing coordination of the sulfur atoms to Au.

For reasons of computational feasibility, the structural optimizations (and calculations of binding energies) are carried out with Au pyramids consisting of 19 atoms for HH and 20 atoms for TT and BB. To ensure a proper description of the Fermi-level alignment in the transport calculations, the gold pyramids are extended to 115 (HH) and 116 (BB, TT) atoms, as displayed in Fig. 3. All added atoms are positioned on the ideal fcc lattice with a lattice constant $a = 0.408$ nm, matching those of the fixed layers for the smaller pyramids. No further geometry optimization is carried out for contacts with extended Au pyramids, and transport properties are computed after a self-consistent, single-point DFT calculation.

IV. THEORETICAL RESULTS

In this section we discuss in detail the effect of different contact geometries on the molecular conformation of the BPDTs and their conduction properties.

A. Molecular conformation

Figure 5 shows the torsion angle between the two phenyl rings for the molecules as determined by x-ray measurements and by DFT calculations in the gas phase as well as in the junction geometries. We notice that gas-phase angles (with SR = H in Fig. 1) generally coincide well with the angles

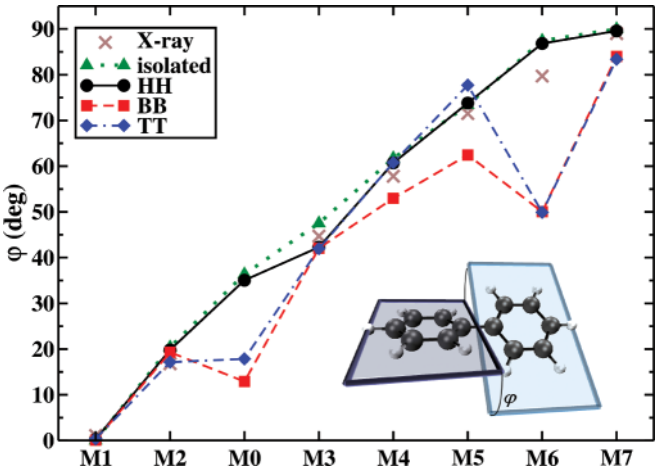

FIG. 5. (Color online) Comparison of the torsion angle φ as determined from x-ray measurements and from DFT calculations in the gas phase (isolated; SR = H in Fig. 1) as well as in the molecular junctions (HH, BB, TT; see Fig. 4).

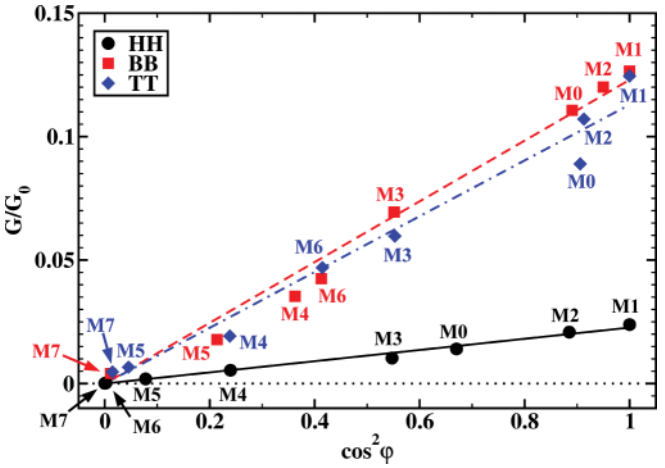

FIG. 6. (Color online) Calculated conductance as a function of $\cos^2\varphi$ for the three types of contact geometries HH, BB, and TT. The angles φ are those of the computed junction geometries. In all cases, lines show best fits for $G = a\cos^2\varphi$ with $a_{HH} = 2.3 \times 10^{-2} G_0$ (solid), $a_{BB} = 1.2 \times 10^{-1} G_0$ (dashed), $a_{TT} = 1.1 \times 10^{-1} G_0$ (dash-dotted).

from the x-ray measurements.[29,33,34] The discrepancy for M6 by roughly 10° has been observed previously.[5] It is likely due to differences between gas-phase and crystal structures caused by the limited stabilization of the conformation, when there is just a single methyl group on each phenyl ring. Note that no x-ray structure measurement exists for M0.

For the contacted molecules deviations of φ from the gas-phase conformation are small for HH, but can be larger for the BB and TT geometries. This is expected from the discussion in Sec. III C. The conformation of the alkyl-bridged BPDTs M1 to M5 is very stable. A slight trend of increasing φ variations for the molecules with the longer, configurationally more flexible alkyl chains can be recognized, however. The torsion angles of M0 and M6 result from the balance between conjugation and modest steric repulsion effects due to H atoms or single CH_3 groups in the orthoposition with respect to the ring-connecting carbons.[19,49,50] Therefore, their φ should be rather sensitive to the geometric constraints in the contacts or the charge transfer between the molecule and the electrodes. As a result, deflections of φ from the gas phase values of up to 40° occur in the calculations. In contrast, the additional methyl side groups in M7 efficiently stabilize φ.[19]

B. Conductance

In Fig. 6 we present the computed conductance values as a function of the torsion angle φ, which the biphenyl molecules adopt in the optimized junction geometries. On the linear conductance scale we find a reasonable $G = a\cos^2\varphi$ dependence for all binding situations with best-fit coefficients[51] $a_{HH} = 2.3 \times 10^{-2} G_0$, $a_{BB} = 1.2 \times 10^{-1} G_0$, $a_{TT} = 1.1 \times 10^{-1} G_0$. This behavior is characteristic for off-resonant charge transport dominated by π-π coupling and is consistent with the experimental observations. Figure 7 shows, for the sample molecule M2, that irrespective of the coordination site, the transport is indeed off-resonant and dominated by the HOMO level.

The results suggest large variations in the conduction properties for the different coordination sites of sulfur to gold. The conductance of junctions with HH geometry is roughly one order of magnitude lower as compared to BB and TT, with the sequence of slopes $a_{HH} \ll a_{TT} \approx a_{BB}$. Similar behavior of the conductance of dithiolated aromatic molecules on binding sites has been reported by other authors.[24,25,27]

For aliphatic alkane molecules, the conductance in the bridge-bonded configuration was reported to be higher than in the top-bonded one.[17] While these findings are compatible with our results in Fig. 6, transport through alkanes is σ-like[17,52,53] and hence differs substantially from the typical π-dominated transport through aromatic molecules. Beside the coordination of the anchoring group the molecular tilt, which determines the overlap of the delocalized π electrons with the electrode, hence plays a crucial role for the conductance of aromatic molecules.[28,54–56] We discuss these aspects further below. However, we note that our contact geometries do not allow us to clearly separate the effects of coordination site and tilt, since both are changed simultaneously.

Junctions of the form HB, HT, etc., should also occur in the experiments. While it would thus be desirable for the comparison between theory and experiment to consider a larger set of junction geometries,[54,57,58] for practical reasons we need to work with a limited one. Since the transport through the junctions is dominated by the molecule, we expect no modification of the $\cos^2\varphi$ law for contact structures with an asymmetric coupling of the BPDT molecules to the gold electrodes.

With regard to absolute values, we observe that the calculated conductances are three (BB and TT geometries) and two (HH geometry) orders of magnitude higher than the experimental ones.[5,29] We attribute this overestimation mostly to the interpretation of Kohn-Sham eigenvalues as approximate quasiparticle energies.[59,60] Since DFT in the generalized gradient approximation generally underestimates the HOMO-LUMO gaps of conjugated organic molecules, transmission resonances are located too close to the metal Fermi energy and molecular junctions are usually too "metallic." However,

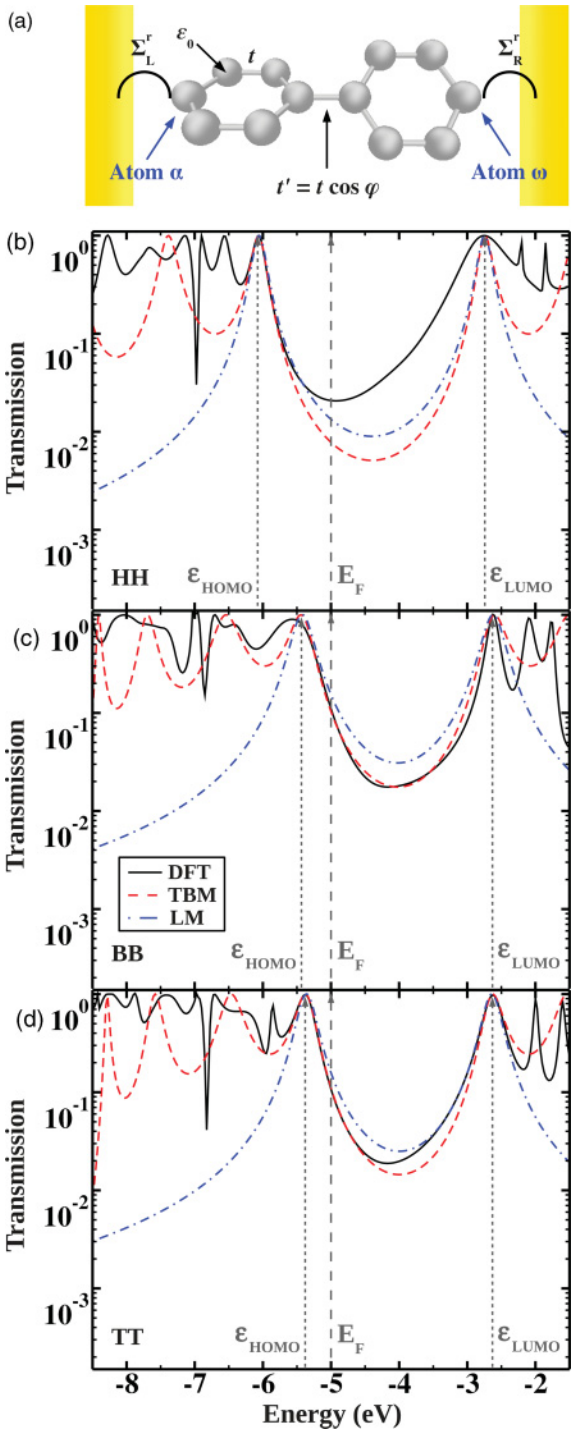

FIG. 7. (Color online) (a) Sketch of the π-orbital TBM used to describe the transport through BPDT molecules. ϵ_0 is the onsite energy, identical for all carbon atoms, t the coupling between nearest-neighbor atoms on each phenyl ring, $t' = t\cos\varphi$ the inter-ring coupling, and φ the torsion angle realized in the particular junction geometry. The terminal atoms of the biphenyl backbone to the left and right are indexed α and ω, respectively, and their couplings to the L,R electrodes are described by the self energies Σ_L^r, Σ_R^r. (b)-(d) Transmission as a function of energy for M2 in the different junction geometries HH, BB, and TT. The solid line is the DFT result, the dashed line the fit with the TBM, and the dash-dotted line corresponds to the LM. Vertical dashed lines indicate, in the order of increasing energy, the position of the HOMO, the Fermi energy, and the LUMO.

also the experimentally measured conductances are subject to uncertainties. Indeed, we compare our results to the "typical" experimental values, as given by the peak positions in room-temperature conductance histograms, and these peaks are rather broad. Variations of molecular conductance, for example, due to interactions of the molecules with the solvent or the influence of vibrations due to finite temperature and current, have not been accounted for in our calculations of static junctions in vacuum.[19,49,50] The differences on a quantitative level remain as a major challenge for future work.

Finally, we note that our calculations do not reproduce the experimental deviation observed for M1.[5] Since φ is unchanged upon contacting (see Fig. 5), we can exclude an explanation based on conformational changes, which would decrease the degree of conjugation and lead to reduced conductances. In spite of the slightly bent structure due to the short CH_2 bridge (see Fig. 1), the intact M1 shows the highest calculated conductance for all coordination geometries (see Fig. 6).

C. Analysis of transmission resonances

In order to understand better the charge transport through the BPDT single-molecule junctions, we analyze the transmission in terms of a TBM and a LM. The physically motivated TBM describes the delocalized π-electron system, relevant for transport away from the perpendicular orientation of the phenyl rings. Based on the simplified Hamiltonian,[30] the transmission is determined by Eq. (A1), and the probability considers the contributions of the individual π orbitals and all interferences between them. In the LM instead, the transmission is approximated as the incoherent sum of transmission resonances originating from individual molecular states. The resonances are assumed to be of a Lorentz form, and the model hence requires the determination of resonance peak positions and their broadenings. For this propose the Lorentzians are often fitted directly to a transmission curve.[31] In order to avoid such a fitting procedure, we derive the parameters of the LM directly from those of the TBM. The procedure is described further below and in Appendix B. Since the molecular frontier orbitals in the BPDT single-molecule contacts dominate the conduction properties, we will concentrate on the HOMO and LUMO resonances only.

We use the TBM of Ref. 30, which is sketched in Fig. 7(a). The Hückel-like, molecular Hamiltonian contains three parameters, namely, the onsite energy ϵ_0 of each carbon atom, the hopping t between nearest-neighbor atoms on each ring, and the torsion angle φ, specific to the considered junction geometry. Together t and φ determine the matrix element between the ring-connecting carbon atoms $t' = t\cos\varphi$. For the description of transport we make use of the wide-band approximation, according to which the retarded self-energy Σ_X^r due to the coupling to the electrode $X = L,R$ is energy independent and determined by the line-broadening matrix Γ_X as $\Sigma_X^r = -i\Gamma_X/2$ [cf. Eq. (A6)]. We assume a symmetric junction $\Gamma = (\Gamma_L)_{\alpha\alpha} = (\Gamma_R)_{\omega\omega}$ and, in line with the nearest-neighbor coupling in the molecule, consider the self-energy to be nonvanishing only on the terminal carbon atoms α and ω of the biphenyl backbone [see Fig. 7(a)]. The TBM is hence

characterized by the four parameters $\varphi, \epsilon_0, t, \Gamma$, where φ is fixed by the considered junction geometry.

To derive the parameters of the LM directly from those of the TBM, we solve the non-Hermitian eigenvalue problem $\sum_k (H + \Sigma^r)_{jk} v_k^\mu = \lambda_\mu v_k^\mu$ and select the complex eigenvalues corresponding to the HOMO and the LUMO. In the eigenvalue equation H_{jk} and $(\Sigma^r)_{jk} = (\Sigma_L^r + \Sigma_R^r)_{jk}$ are the Hamiltonian matrix and the self-energy matrix of the TBM, respectively, and $\lambda_\mu = \epsilon_\mu - i\gamma_\mu$. We measure the real part of the complex eigenvalues with respect to the Fermi energy, introducing $\tilde{\epsilon}_H = \epsilon_{\mathrm{HOMO}} - E_F$ and $\tilde{\epsilon}_L = \epsilon_{\mathrm{LUMO}} - E_F$. Due to the symmetries of the TBM we find for the imaginary parts $\gamma_{\mathrm{HOMO}} = \gamma_{\mathrm{LUMO}}$, and set $\tilde{\Gamma} = \gamma_{\mathrm{HOMO}}$. From the relation between the TBM and the LM discussed in Appendix B [see Eq. (B2)], we can identify $\tilde{\Gamma}$ with the width of the Lorentzian transmission resonances related to the HOMO and the LUMO. Finally, we determine the transmission for the LM via Eq. (B2) as a sum over these two frontier orbitals only. The LM is thus characterized by $\tilde{\epsilon}_H, \tilde{\epsilon}_L, \tilde{\Gamma}$ and is specific to a certain molecule and junction geometry, as described by $\varphi, \epsilon_0, t, \Gamma$ in the TBM.

Using the TBM, we have fitted the transmission $\tau(E)$ of the well-conjugated molecules M1–M4, as determined by the DFT calculations. Setting φ to the value of the torsion angle realized in the particular junction geometry, we place special emphasis on a good fit in the region of the HOMO-LUMO gap. When such a fit is too ambitious due to the simplicity of the TBM, we describe well at least the region between the HOMO and E_F, to determine effective parameters for the dominant transmission resonance, as well as the position of the LUMO peak. In this way, we obtain the values for ϵ_0, t, Γ given in Table I. Specific LM parameters for M2 are provided in the same table, and DFT, TBM, and LM transmission curves for M2 are shown in Fig. 7(b)–7(d).

The differences between the curves of the TBM and the LM in Fig. 7(b)–7(d) in the region of the HOMO-LUMO gap illustrate approximations related to the neglect of interference effects in the LM. Indeed, we find that the transmission is slightly overestimated when it is regarded as the superposition of incoherent transmission resonances. In the following we restrict our discussion to the parameters of the LM for M2, since they are easy to interpret and those of the generic TBM contain similar information for our present purposes.

The data in Table I show very similar values of $\tilde{\Gamma}^{M2}$ for the different junction geometries. While the increasing line width $\tilde{\Gamma}^{M2}$ when going from TT to BB is consistent with the expectation of a better electronic coupling for a higher coordination of the sulfur atom, the molecular tilt also plays a role. The perpendicular orientation of the BPDTs for geometry HH thus leads to a reduced $\tilde{\Gamma}^{M2}$. As an important conclusion, the values of $\tilde{\epsilon}_H^{M2}$ and $\tilde{\epsilon}_L^{M2}$ show that the HOMO is closer to E_F than the LUMO by more than 1 eV. In addition, the reduced conductance for HH in Fig. 6 is explained by the HOMO level being around 0.5 eV further away from E_F than for BB and TT.

We attribute the shift of the HOMO level toward lower energies for increasing coordination number of the sulfur atoms to the different amounts of transferred charge at the molecule-Au interface. Indeed, both Löwdin and electrostatic-potential-derived charges yield a leakage of electrons from the molecule, including the S atoms, to the Au electrodes, when going from TT over BB to the HH geometry. Variations of the conductance therefore mostly arise from changes in the alignment of the HOMO level with respect to the Fermi energy of the Au electrodes, and originate from charge redistributions, which are sensitive to the coordination site of the sulfur atom at the molecule-electrode interface.

TABLE I. Parameters ϵ_0, t, Γ of the TBM obtained by fitting the DFT-based $\tau(E)$ curves for M1–M4. The parameters $\tilde{\epsilon}_H^{M2}, \tilde{\epsilon}_L^{M2}, \tilde{\Gamma}^{M2}$ of the LM are those derived from the TBM for M2. All values are given in units of eV.

	ϵ_0	t	Γ	$\tilde{\epsilon}_H^{M2}$	$\tilde{\epsilon}_L^{M2}$	$\tilde{\Gamma}^{M2}$
HH	−4.40	−2.30	0.70	−1.05	2.25	0.11
BB	−4.02	−1.95	1.10	−0.42	2.38	0.18
TT	−4.00	−1.90	0.96	−0.36	2.36	0.15

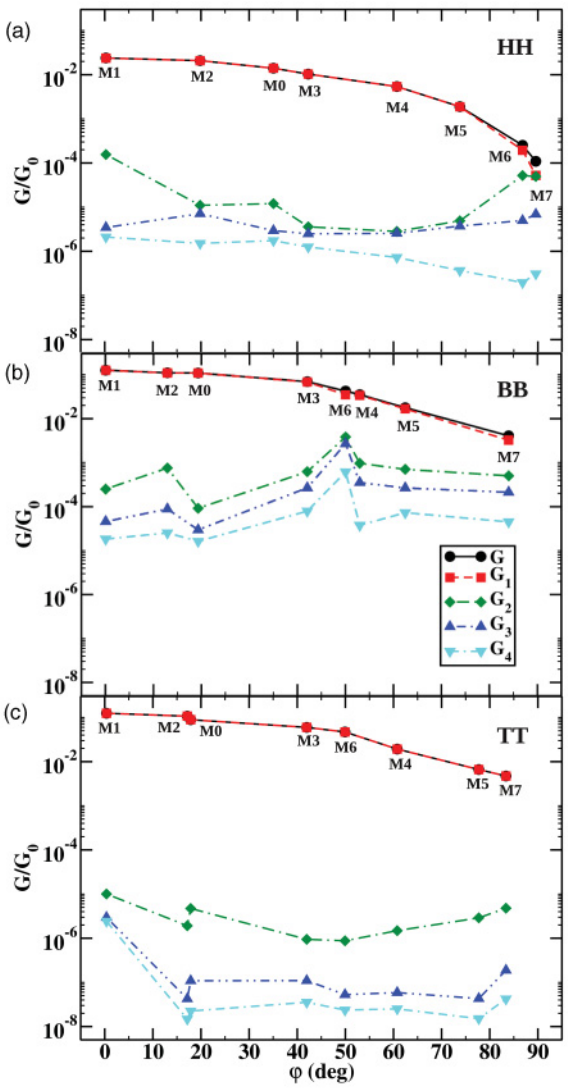

FIG. 8. (Color online) Calculated conductance G and the conductance $G_n = G_0 \tau_n(E_F)$ with $n = 1, \ldots, 4$ of the four transmission eigenchannels with the highest contribution to G for the set of BPDTs in (a) HH, (b) BB, and (c) TT configurations.

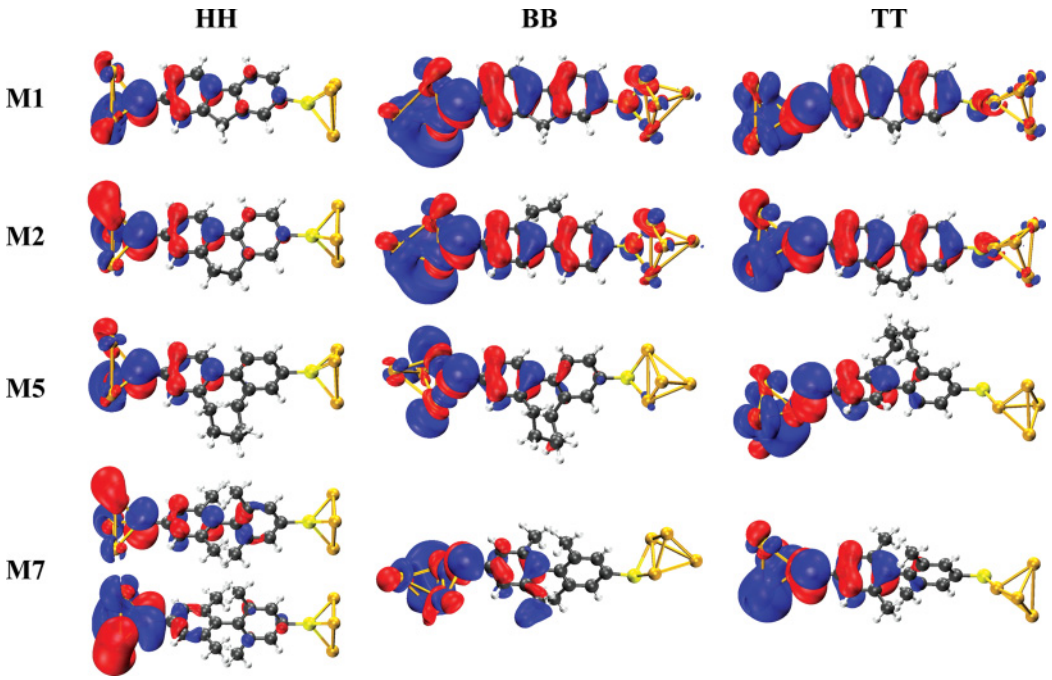

FIG. 9. (Color online) Wave function of the dominant, left-incoming transmission eigenchannel for selected BPDT molecules in the HH, BB, and TT geometries. The same isosurface value of the wave functions is used in all the plots to allow for their comparison. However, the isosurface value has been reduced by a factor of 4 on the right phenyl ring of M7 for HH to visualize the π-σ and σ-π character of the two eigenchannel wave functions, which yield the same contribution to the conductance.

D. Transmission eigenchannels

To explore further the electron transport through BPDT molecules, especially for the situation $\varphi \simeq 90^\circ$ where the TBM looses its validity, we consider the eigenchannel decomposition of the conductance and the corresponding wave functions. The results are displayed in Figs. 8 and 9.

We observe one dominant eigenchannel, whose transmission probability is decreasing gradually with increasing torsion angle for geometries with $\varphi \lesssim 80^\circ$ (Fig. 8). The wave function of this channel is formed from those p orbitals of the C atoms, which are perpendicular to the phenyl-ring planes (see the results for M1 and M2 in Fig. 9). The resulting π orbitals, which comprise the terminal thiol groups, hence exhibit nodes in the ring planes. The findings agree with the expectation that for the small torsion angles, resulting in a high degree of conjugation, electric transport should occur via the delocalized π-electron system of the BPDTs.

The π-π coupling between the rings is suppressed for $\varphi \approx 90^\circ$, since it varies as $\cos\varphi$.[19,20,25] In this case the molecular states become more localized on the individual rings. The incoming Bloch waves from the leads can still couple through the sulfur linker atom into the π-electron system of one of the rings, but they are back-reflected at the ring-connecting carbon atom. This results in a large suppression of the transmission (Fig. 8) and becomes manifest in a low amplitude of the wave function on the second ring (see the results for M5 and M7 in Fig. 9). In this regime the π-σ coupling, proportional to $\sin\varphi$, dominates.[20,25] The σ character of the wave functions is apparent from the absence of nodal planes in the phenyl ring planes and the high amplitude of the eigenchannel wave function on the axis that connects the neighboring carbon atoms.

The isolated biphenyl molecules M0 and M7 (SR = H in Fig. 1) with φ set to 90° possess D_{2d} symmetry. Then σ-π and π-σ orbitals are degenerate, which should lead to two dominant transmission eigenchannels with the same contribution to the conductance.[20,25] However, the presence of the electrodes generally leads to a low symmetry of the junction as a whole and may also modify the molecular geometry. Hence, it is interesting to analyze the degeneracy of eigenchannels in the different coordination geometries for M7 with the nearly perpendicular gas phase torsion angle. Using the ratio of the channel conductances G_2/G_1 with $G_n = G_0\tau_n(E_F)$ as a measure for the degeneracy, we find the values given in Table II.

The data in Table II demonstrate the general absence of the channel degeneracy and a high sensitivity of G_2/G_1 to the junction geometry. Only for the HH contact geometry do we find a nearly perfect degeneracy of the two dominant transmission eigenchannels. Consistent with this, Fig. 9 demonstrates that their wave functions are indeed of π-σ and σ-π type. The degeneracy can be explained by the fact that M7 in the HH geometry stands perpendicular to the electrodes. The torsion angle of the contacted molecule is hence close to those in the gas phase (see Fig. 5), and the overlap of the

TABLE II. Ratio G_2/G_1 of the highest eigenchannel contributions to the conductance for M7 in the three junction geometries studied.

	HH	BB	TT
M7	0.95	0.15	1.0×10^{-3}

molecular π orbitals with the electrode states is such that the degeneracy of molecular orbitals is not strongly lifted. Therefore, the transmission reflects symmetry properties of the molecule. For the BB and TT junctions, deviations from the channel degeneracy result from the geometric constraints set by the electrodes, which cause φ in the junctions to deviate from 90°, and from the asymmetric overlap of the molecular π states with the electrode states to the left and right (see also Sec. III C). Contact structures with a different coordination of the sulfur atoms at the left and right electrodes would only enhance the asymmetry effects. Thus, our results clearly show that the reduced symmetry of the complete junction has to be considered for transport and not just the symmetry of the isolated molecule alone.[61]

These findings suggest that measurements of the transmission eigenchannel degeneracy may serve as a sensitive probe to determine the coordination geometry in biphenyl-type single-molecule junctions. However, there are several factors not included in our idealized treatment. Thus, it would be interesting to study how strongly a finite bias voltage will lift an existing π-σ and σ-π channel degeneracy by breaking of the left-right symmetry. Furthermore, also dynamic effects due to vibrational modes and Jahn-Teller distortions should lead to an effective splitting of the pair of degenerate eigenchannels. In addition to these issues, it remains an experimental challenge to determine the conduction eigenchannel transparencies for contacts with a low transmission, since the existing techniques, employing superconducting electrodes[14] or shot noise,[15] yield very low signals in such situations.

Our calculations illustrate that the alkyl chains do not participate significantly in transport, as expected from the large gaps between HOMO and LUMO levels of alkanes.[17] Considering the dominant transmission eigenchannels in Fig. 9, we see that there is indeed practically no weight of the wave function on the alkyl chain, even for the short chains present in M1 and M2.

V. CONCLUSIONS

Motivated by recent experiments,[5,29] we have presented a detailed theoretical analysis of the charge transport properties of Au-BPDT-Au single-molecule junctions. The three types of contact geometries in our DFT-based study differed in essential aspects at the molecule-metal interface. They were mainly the coordination site of the anchoring sulfur atoms and the tilt of the molecule with respect to the electrodes. Given the extensive statistical analysis in the experiments, this set of geometries is clearly very limited. Furthermore, without an analysis of the junction formation process, it is difficult to make a statement on the probability of their occurrence. However, we hope that they can be used to describe general trends, such as the influence of molecular conformation on conductance and the variability of transport properties with contact geometry.

We have investigated electrode-induced changes of the molecular conformation due to charge transfer and geometric constraints and find that they are rather small for most molecules and types of junctions considered here. Compared to the somewhat larger variations for M0 and M6, whose φ is not fixed by an alkyl strap or strong steric effects, our calculations show that the appropriate design of the side groups can help to stabilize the torsion angle.

The transport calculations confirm a $\cos^2\varphi$ dependence of the conductance for the well-conjugated molecules in each type of junction geometry. This is in accordance with the experimental observations and is characteristic for off-resonant transport through the π-electron system.[19] For biphenyl molecules with torsion angles close to the perpendicular orientation, however, we observe systematic deviations in our experimental data from the $\cos^2\varphi$ law predicted by a simplified π-orbital TBM. In that regime of a broken conjugation, our analysis of DFT-based transmission eigenchannel wave functions reveals residual conductance contributions from a pair of π-σ-type conduction channels.

Finally, our calculations suggest that molecular junctions with sulfur atoms bound to the "hollow" site of gold electrodes could exhibit an order-of-magnitude smaller conductance as compared to junctions with sulfur atoms bound via "top" or "bridge" sites. Our analysis shows that the transport is dominated by the molecular HOMO level in all cases, and variations of the conductance arise from changes in the alignment of that level with respect to the Fermi energy of the Au electrodes. These changes in turn originate from the charge transfer between the molecule and the electrode, which is sensitive to the coordination site of the sulfur atom.

ACKNOWLEDGMENTS

We acknowledge fruitful discussions with A. Bagrets, F. Evers, and V. Meded. R. Ahlrichs and M. Sierka are thanked for providing us with TURBOMOLE. M.B. and G.S. were supported through the DFG Center for Functional Nanostructures (Project C3.6), the DFG priority program 1243, and the Initial Training Network "NanoCTM" (Grant No. FP7-PEOPLE-ITN-2008-234970), F.P. through the Young Investigator Group, and J.K.V. through the Academy of Finland. D.V. and M.M. acknowledge funding by the Swiss National Science Foundation and the Swiss National Center of Competence in Research "Nanoscale Science." The work of A.M. and T.W. was financed by the Swiss National Science Foundation (200021.124643, NFP62), the Initial Training Network FUNMOLS, the DFG priority program 1243, and the University of Bern.

APPENDIX A: DETERMINATION OF TRANSMISSION EIGENCHANNELS

In this Appendix, we provide further details on how we determine the transmission eigenchannels, in particular their wave functions. The result is equivalent to that of Ref. 32. However, our procedure avoids the Löwdin orthogonalizations and uses, instead, a consistent formulation in terms of nonorthogonal basis states. This reduces the numerical effort and eliminates possible numerical instabilities resulting from the forward and backward Löwdin transformations. Isosurfaces of eigenchannel wave functions employing this scheme are plotted in Fig. 9.

To compute the charge transport, we divide the nanocontact into a L, C, and R region (see Fig. 3) and classify the states of our local, nonorthogonal basis $|e_i\rangle$ accordingly. The C region

is assumed to be long enough to neglect the elements $H_{LR} = H_{RL}^T$ and $S_{LR} = S_{RL}^T$ of the real and symmetric Hamiltonian $H_{jk} = \langle e_j|\breve{H}|e_k\rangle$ and overlap $S_{jk} = \langle e_j|e_k\rangle$. Here $\breve{H}$ is the Hamiltonian operator in the combined L,C,R space.

Adopting a notation along the lines of Refs. 32 and 47, we express the energy-dependent transmission as

$$\tau(E) = \mathrm{Tr}[A_L(E)\Gamma_R(E)], \tag{A1}$$

where we define the spectral function

$$A_X(E) = G^r_{CC}(E)\Gamma_X(E)G^a_{CC}(E). \tag{A2}$$

Here and below, X stands for either L or R ($X = L,R$). $A_X(E)$ is the contribution to the full spectral density of C from scattering states originating in lead X.[32] In the expression,

$$G^r_{CC}(E) = \left[(E+i\eta)S_{CC} - H_{CC} - \Sigma^r_L(E) - \Sigma^r_R(E)\right]^{-1} \tag{A3}$$

is the retarded Green's function of the device (or C region), with $\eta > 0$ an infinitesimal constant, and $G^a_{CC} = (G^r_{CC})^\dagger$ is the advanced function. For G^r_{CC} we need the self-energies

$$\Sigma^r_X(E) = (H_{CX} - ES_{CX})g^r_{XX}(E)(H_{XC} - ES_{XC}), \tag{A4}$$

where

$$g^r_{XX}(E) = [(E+i\eta)S_{XX} - H_{XX}]^{-1} \tag{A5}$$

is the retarded Green's function of region X. The matrix

$$\Gamma_X(E) = -2\mathrm{Im}\left[\Sigma^r_X(E)\right] \tag{A6}$$

is the line-broadening matrix. Note that both matrices $A_X(E)$ and $\Gamma_X(E)$ are positive-semidefinite. For notational convenience, we will henceforth suppress the energy dependence of the quantities.

In the following we use a basis-independent notation with operators such as $\hat{A}_L$ and $\hat{\Gamma}_R$, which are defined by their matrix elements in the C space. We also assume the existence of a dual basis $|e^j\rangle$, satisfying $\langle e^j|e_k\rangle = \delta_{jk}$ and $\hat{1} = \sum_{j\in C}|e^j\rangle\langle e_j|$. Now let $(A_L)^{jk} = \langle e^j|\hat{A}_L|e^k\rangle$ and $(\Gamma_R)_{jk} = \langle e_j|\hat{\Gamma}_R|e_k\rangle$. The matrix elements $(\Gamma_R)_{jk}$ are the components of Eq. (A6). They are "covariant," since the factors $H_{jk} - ES_{jk}$ in Eq. (A4) are covariant. The elements $(A_L)^{jk}$ are also just the components of Eq. (A2). However, they are "contravariant" since the Green's functions G^a_{CC} and G^r_{CC} [see Eq. (A3)] are defined as the inverse of covariant matrices, i.e., $\sum_k[(E \pm i\eta)S_{jk} + H_{jk}]\langle e^k|\breve{G}^{r,a}|e^l\rangle = \delta_{jl}$.

Motivated by Eq. (A1) we also define the transmission probability operator

$$\hat{T}_1 = \hat{A}_L\hat{\Gamma}_R. \tag{A7}$$

We will now show how the eigenchannel wave functions for waves coming in from the left are conveniently obtained from the right eigenvectors of $\hat{T}_1$ in the nonorthogonal basis by slightly reformulating the procedure presented in Ref. 32.

Consider the eigenvalue equation

$$\hat{A}_L|\chi_j\rangle = \lambda_j|\chi_j\rangle. \tag{A8}$$

The eigenvectors $|\chi_j\rangle$ of the Hermitian operator $\hat{A}_L$ are orthonormal ($\langle\chi_j|\chi_k\rangle = \delta_{jk}$). Using them we define the states $|\tilde{\chi}_j\rangle = \sqrt{\frac{\lambda_j}{2\pi}}|\chi_j\rangle$ and the corresponding dual ones $|\tilde{\chi}^j\rangle = \sqrt{\frac{2\pi}{\lambda_j}}|\chi_j\rangle$ (for all $\lambda_j \neq 0$) so that $\langle\tilde{\chi}^j|\tilde{\chi}_k\rangle = \delta_{jk}$. It was shown in Ref. 32 that the states $|\tilde{\chi}_j\rangle$ are the device part of orthogonal linear combinations of energy-normalized scattering states, describing waves coming in from the left lead. The transmission eigenchannels $|\phi_n\rangle$ can be expanded as

$$|\phi_n\rangle = \sum_j|\tilde{\chi}_j\rangle c_{jn}, \tag{A9}$$

with $c_{jn} = \langle\tilde{\chi}^j|\phi_n\rangle$. The coefficients in this expansion may be found from the eigenvalue equation

$$\hat{T}_1|\phi_n\rangle = \tau_n|\phi_n\rangle. \tag{A10}$$

Multiplying by $\langle\tilde{\chi}^j|$ on the left and using Eqs. (A8)–(A9), this results in[32]

$$2\pi\sum_k\langle\tilde{\chi}_j|\hat{\Gamma}_R|\tilde{\chi}_k\rangle c_{kn} = \tau_n c_{jn}. \tag{A11}$$

Employing the normalization condition $\sum_k c^*_{kj}c_{kl} = \delta_{jl}$, the linear combination of Eq. (A9) preserves the energy normalization of the left-incoming states. For $\langle\tilde{\chi}_j|\hat{\Gamma}_R|\tilde{\chi}_m\rangle = \sum_{k,l}\tilde{d}^*_{kj}(\Gamma_R)_{kl}\tilde{d}_{lm}$ the coefficients $\tilde{d}_{lm} = \langle e^l|\tilde{\chi}_m\rangle = \sqrt{\frac{\lambda_m}{2\pi}}d_{lm}$ are determined from $\hat{A}_L$ by multiplying Eq. (A8) by $\langle e_j|$ on the left and inserting $\hat{1}$. This leads to the generalized eigenvalue problem

$$\sum_{k,l,m}S_{jk}(A_L)^{kl}S_{lm}d_{mn} = \lambda_n\sum_k S_{jk}d_{kn}, \tag{A12}$$

with $d_{mn} = \langle e^m|\chi_n\rangle$ and $\sum_{k,l}d^*_{kj}S_{kl}d_{lm} = \delta_{jm}$.

Putting these results together, the explicit form of the eigenchannel wave function for region C in terms of the basis functions is obtained from

$$\langle\vec{r}|\phi_n\rangle = \sum_{j,k}\langle\vec{r}|e_j\rangle\tilde{d}_{jk}c_{kn}. \tag{A13}$$

Using Eqs. (A3)–(A6) and (A11)–(A13) the transmission eigenchannel wave function can be computed without resorting to a Löwdin transformation.

We note that the eigenvalues τ_n of $\hat{T}_1$ in Eq. (A10) are real, since $\hat{\Gamma}_R$ is a Hermitian operator [see Eq. (A11)]. It is also easy to show that they agree with the eigenvalues of more symmetric, Hermitian transmission operators of the form $\hat{T}_2 = \hat{t}\hat{t}^\dagger$. Given $|\phi_n\rangle$ and τ_n from Eq. (A10) and assuming, e.g., $\hat{t} = \sqrt{\hat{\Gamma}_R}\hat{G}^r\sqrt{\hat{\Gamma}_L}$, the states $|\phi'_n\rangle = \sqrt{\hat{\Gamma}_R}|\phi_n\rangle$ are eigenstates of $\hat{T}_2$ with the eigenvalues $\tau'_n = \tau_n$. Furthermore, it is easy to prove[46] that the eigenvalues satisfy $0 \leqslant \tau_n \leqslant 1$, as expected for transmission probabilities.

APPENDIX B: RELATION BETWEEN THE TIGHT-BINDING AND LORENTZ MODEL

The LM is frequently used to describe the transmission in the field of molecular electronics. Typically, a Lorentzian function is fitted to the resonance dominating the transmission at the Fermi energy. Here we discuss in which situation the LM coincides with the TBM.

We consider the non-Hermitian eigenvalue problem $(\hat{H}+\hat{\Sigma}^r)|\mu\rangle=\lambda_\mu|\mu\rangle$ with $\lambda_\mu=\epsilon_\mu-i\gamma_\mu$, the symmetric and Hermitian Hamilton operator $\hat{H}$, and the symmetric, but non-Hermitian retarded self-energy operator $\hat{\Sigma}^r=\hat{\Sigma}^r_L+\hat{\Sigma}^r_R$ composed of contributions from the L and R electrodes. By $\langle\tilde{\mu}|$ we denote the left eigenstate with the same eigenvalue λ_μ as the corresponding right eigenstate $|\mu\rangle$, i.e., $\langle\tilde{\mu}|(\hat{H}+\hat{\Sigma}^r)=\lambda_\mu\langle\tilde{\mu}|$. The C region is assumed to be identical to the molecule in the TBM [see Fig. 7(a)]. Using the spectral decomposition of the Green's function in the expression for the energy-dependent transmission $\tau(E)$ [see Eqs. (A1) and (A2)], we obtain

$$\tau(E)=\sum_{\mu,\nu}\frac{\langle\tilde{\mu}|\hat{\Gamma}_L|\nu\rangle\langle\tilde{\nu}|\hat{\Gamma}_R|\mu\rangle}{(E-\epsilon_\mu+i\gamma_\mu)(E-\epsilon_\nu-i\gamma_\nu)}, \tag{B1}$$

where the sum is over all those eigenstates $|\mu\rangle$ of the biphenyl that obtain a finite line width $\gamma_\mu\neq 0$ by the coupling to the electrodes and that hence contribute to the transport.

Let us now make the wide-band approximation and consider the energy-independent expression $\hat{\Sigma}^r=-i(\hat{\Gamma}_L+\hat{\Gamma}_R)/2$ to be a small perturbation. Within lowest-order perturbation theory we obtain $\lambda_\mu=\epsilon^0_\mu-i\gamma_\mu$ with $\hat{H}|\mu^0\rangle=\epsilon^0_\mu|\mu^0\rangle$ and $\gamma_\mu=i\langle\mu^0|\hat{\Sigma}^r|\mu^0\rangle$. Additionally, we assume a symmetric coupling $(\Gamma_L)_{\alpha\alpha}=(\Gamma_R)_{\omega\omega}=\Gamma$, where the indices α,ω refer to those atoms of the biphenyl backbone that are closest to the L,R electrodes [see Fig. 7(a)] and where local basis states are understood to be orthogonal in the spirit of the Hückel approximation. By exploiting the inversion symmetry of the TBM, it follows that $\gamma_\mu=\langle\mu^0|\hat{\Gamma}_X|\mu^0\rangle$ since $\hat{M}^2=\hat{1}$, $\hat{M}\hat{H}\hat{M}=\hat{H}$, and $\hat{M}\hat{\Gamma}_L\hat{M}=\hat{\Gamma}_R$ with the operator $\hat{M}=\hat{M}^\dagger$ describing the inversion of the molecule.

The perturbation theory is valid in the regime $\Gamma\ll t,t'$, where t and t' determine the separation between the resonance energies ϵ_μ relevant for transport. When they are well separated, the largest contributions to the transmission in Eq. (B1) arise when $\mu=\nu$, since cross-terms are suppressed by a large off-resonant denominator. In this case the transmission is well represented as the sum of incoherent Lorentz resonances

$$\tau(E)\approx\sum_\mu\frac{\gamma_\mu^2}{(E-\epsilon_\mu)^2+\gamma_\mu^2}, \tag{B2}$$

and the TBM simplifies to the LM.

*marcel.mayor@unibas.ch
†thomas.wandlowski@dcb.unibe.ch
‡fabian.pauly@kit.edu

[1] M. A. Reed, C. Zhou, C. J. Muller, T. P. Burgin, and J. M. Tour, Science **278**, 252 (1997).
[2] J. Reichert, R. Ochs, D. Beckmann, H. B. Weber, M. Mayor, and H. v. Löhneysen, Phys. Rev. Lett. **88**, 176804 (2002).
[3] B. Xu and N. J. Tao, Science **301**, 1221 (2003).
[4] L. Venkataraman, J. E. Klare, C. Nuckolls, M. S. Hybertsen, and M. L. Steigerwald, Nature (London) **442**, 904 (2006).
[5] A. Mishchenko, D. Vonlanthen, V. Meded, M. Bürkle, C. Li, I. V. Pobelov, A. Bagrets, J. K. Viljas, F. Pauly, F. Evers, M. Mayor, and T. Wandlowski, Nano Lett. **10**, 156 (2010).
[6] A. Mishchenko, L. A. Zotti, D. Vonlanthen, M. Bürkle, F. Pauly, J. C. Cuevas, M. Mayor, and T. Wandlowski, J. Am. Chem. Soc. **133**, 184 (2011).
[7] S. Wu, M. T. Gonzalez, R. Huber, S. Grunder, M. Mayor, C. Schönenberger, and M. Calame, Nat. Nanotechnol. **3**, 569 (2008).
[8] L. Lafferentz, F. Ample, H. Yu, S. Hecht, C. Joachim, and L. Grill, Science **323**, 1193 (2009).
[9] S. J. van der Molen, J. Liao, T. Kudernac, J. S. Agustsson, L. Bernard, M. Calame, B. J. van Wees, B. L. Feringa, and C. Schönenberger, Nano Lett. **9**, 76 (2009).
[10] R. H. M. Smit, Y. Noat, C. Untiedt, N. D. Lang, M. C. van Hemert, and J. M. van Ruitenbeek, Nature (London) **419**, 906 (2002).
[11] Z. Ioffe, T. Shamai, A. Ophir, G. Noy, I. Yutsis, K. Kfir, O. Cheshnovsky, and Y. Selzer, Nat. Nanotechnol. **3**, 727 (2008).
[12] D. R. Ward, D. A. Corley, J. M. Tour, and D. Natelson, Nat. Nanotechnol. **6**, 33 (2011).
[13] P. Reddy, S.-Y. Jang, R. A. Segalman, and A. Majumdar, Science **315**, 1568 (2007).
[14] E. Scheer, N. Agraït, J. C. Cuevas, A. L. Yeyati, B. Ludoph, A. Martin-Rodero, G. R. Bollinger, J. M. van Ruitenbeek, and C. Urbina, Nature (London) **394**, 154 (1998).
[15] M. Kiguchi, O. Tal, S. Wohlthat, F. Pauly, M. Krieger, D. Djukic, J. C. Cuevas, and J. M. van Ruitenbeek, Phys. Rev. Lett. **101**, 046801 (2008).
[16] L. Venkataraman, J. E. Klare, I. W. Tam, C. Nuckolls, M. S. Hybertsen, and M. L. Steigerwald, Nano Lett. **6**, 458 (2006).
[17] C. Li, I. Pobelov, T. Wandlowski, A. Bagrets, A. Arnold, and F. Evers, J. Am. Chem. Soc. **130**, 318 (2008).
[18] M. P. Samanta, W. Tian, S. Datta, J. I. Henderson, and C. P. Kubiak, Phys. Rev. B **53**, R7626 (1996).
[19] F. Pauly, J. K. Viljas, J. C. Cuevas, and G. Schön, Phys. Rev. B **77**, 155312 (2008).
[20] F. Pauly, J. K. Viljas, and J. C. Cuevas, Phys. Rev. B **78**, 035315 (2008).
[21] H. Kondo, J. Nara, H. Kino, and T. Ohno, Jpn. J. Appl. Phys. **47**, 4792 (2008).
[22] C. M. Finch, S. Sirichantaropass, S. W. Bailey, I. M. Grace, V. M. García-Suárez, and C. J. Lambert, J. Phys. Condens. Matter **20**, 022203 (2008).
[23] G. C. Solomon, D. Q. Andrews, R. P. Van Duyne, and M. A. Ratner, ChemPhysChem **10**, 257 (2009).
[24] Y. Xue and M. A. Ratner, Phys. Rev. B **68**, 115407 (2003).
[25] J. Tomfohr and O. F. Sankey, J. Chem. Phys. **120**, 1542 (2004).
[26] H. Basch, R. Cohen, and M. A. Ratner, Nano Lett. **5**, 1668 (2005).
[27] Z. Li and D. S. Kosov, Phys. Rev. B **76**, 035415 (2007).
[28] S. Y. Quek, M. Kamenetska, M. L. Steigerwald, H. J. Choi, S. G. Louie, M. S. Hybertsen, J. B. Neaton, and L. Venkataraman, Nat. Nanotechnol. **4**, 230 (2009).
[29] D. Vonlanthen, A. Mishchenko, M. Elbing, M. Neuburger, T. Wandlowski, and M. Mayor, Angew. Chem., Int. Ed. **48**, 8886 (2009).
[30] J. K. Viljas, F. Pauly, and J. C. Cuevas, Phys. Rev. B **77**, 155119 (2008).
[31] M. Paulsson and S. Datta, Phys. Rev. B **67**, 241403 (2003).

[32]M. Paulsson and M. Brandbyge, Phys. Rev. B **76**, 115117 (2007).
[33]A. Shaporenko, M. Elbing, A. Błaszczyk, C. von Hänisch, M. Mayor, and M. Zharnikov, J. Phys. Chem. B **110**, 4307 (2006).
[34]D. Vonlanthen, J. Rotzler, M. Neuburger, and M. Mayor, Eur. J. Org. Chem. 120 (2010).
[35]D. Vonlanthen, A. Rudnev, A. Mishchenko, A. Käslin, J. Rotzler, M. Neuburger, T. Wandlowski, and M. Mayor, Chem. Eur. J. **17**, 7236 (2011).
[36]J. A. Malen, P. Doak, K. Baheti, T. D. Tilley, A. Majumdar, and R. A. Segalman, Nano Lett. **9**, 3406 (2009).
[37]J. Rotzler, H. Gsellinger, M. Neuburger, D. Vonlanthen, D. Haussinger, and M. Mayor, Org. Biomol. Chem. **9**, 86 (2011).
[38]L. Venkataraman, Y. S. Park, A. C. Whalley, C. Nuckolls, M. S. Hybertsen, and M. L. Steigerwald, Nano Lett. **7**, 502 (2007).
[39]Similar results for experiments at a different BPDT concentration for selected molecules (0.25 mM) exclude an influence of intermolecular interactions on conductance.
[40]R. Ahlrichs, M. Bär, M. Häser, H. Horn, and C. Kölmel, Chem. Phys. Lett. **162**, 165 (1989).
[41]A. Schäfer, C. Huber, and R. Ahlrichs, J. Chem. Phys. **100**, 5829 (1994).
[42]K. Eichkorn, O. Treutler, H. Öhm, M. Häser, and R. Ahlrichs, Chem. Phys. Lett. **242**, 652 (1995).
[43]K. Eichkorn, F. Weigend, O. Treutler, and R. Ahlrichs, Theor. Chem. Acc. **97**, 119 (1997).
[44]A. D. Becke, Phys. Rev. A **38**, 3098 (1988).
[45]J. P. Perdew, Phys. Rev. B **33**, 8822 (1986).
[46]S. Datta, *Electronic Transport in Mesoscopic Systems* (Cambridge University Press, Cambridge, 1997).
[47]F. Pauly, J. K. Viljas, U. Huniar, M. Häfner, S. Wohlthat, M. Bürkle, J. C. Cuevas, and G. Schön, New J. Phys. **10**, 125019 (2008).
[48]A. Bagrets, N. Papanikolaou, and I. Mertig, Phys. Rev. B **75**, 235448 (2007).
[49]J.-T. Lü, M. Brandbyge, and P. Hedegård, Nano Lett. **10**, 1657 (2010).
[50]V. Fatemi, M. Kamenetska, J. B. Neaton, and L. Venkataraman, Nano Lett. **11**, 1988 (2011).
[51]We note that small differences in the slope values a as compared to Ref. 5 arise from the study of a different junction geometry for TT and a slightly modified ECC for BB.
[52]C. R. Arroyo, T. Frederiksen, G. Rubio-Bollinger, M. Vélez, A. Arnau, D. Sánchez-Portal, and N. Agraït, Phys. Rev. B **81**, 075405 (2010).
[53]Y. Kim, T. J. Hellmuth, M. Bürkle, F. Pauly, and E. Scheer, ACS Nano **5**, 4104 (2011).
[54]Y. Hu, Y. Zhu, H. Gao, and H. Guo, Phys. Rev. Lett. **95**, 156803 (2005).
[55]W. Haiss, C. Wang, R. Jitchati, I. Grace, S. Martín, A. S. Batsanov, S. J. Higgins, M. R. Bryce, C. J. Lambert, P. S. Jensen, and R. J. Nichols, J. Phys. Condens. Matter **20**, 374119 (2008).
[56]I. Diez-Perez, J. Hihath, T. Hines, Z.-S. Wang, G. Zhou, K. Mullen, and N. Tao, Nat. Nanotechnol. **6**, 226 (2011).
[57]M. Paulsson, C. Krag, T. Frederiksen, and M. Brandbyge, Nano Lett. **9**, 117 (2008).
[58]F. Pauly, M. Dreher, J. K. Viljas, M. Häfner, J. C. Cuevas, and P. Nielaba, Phys. Rev. B **74**, 235106 (2006).
[59]S. Y. Quek, L. Venkataraman, H. J. Choi, S. G. Louie, M. S. Hybertsen, and J. B. Neaton, Nano Lett. **7**, 3477 (2007).
[60]M. Strange, C. Rostgaard, H. Häkkinen, and K. S. Thygesen, Phys. Rev. B **83**, 115108 (2011).
[61]G. C. Solomon, A. Gagliardi, A. Pecchia, T. Frauenheim, A. D. Carlo, J. R. Reimers, and N. S. Hush, J. Chem. Phys. **125**, 184702 (2006).